Dyes and Pigments 198 (2022) 109939

Contents lists available at ScienceDirect

Dyes and Pigments

journal homepage: www.elsevier.com/locate/dyepig

AIEgens with cyano-modification in different sites: Potential 'Meta-site effect' in mechanochromism behavior

Mengshi Wang [a], Yuanheng Wang [b], Renjian Hu [a], Ruoxin Li [a], Zhigang Shuai [b], Yen Wei [a,c,*]

[a] The Key Laboratory of Bioorganic Phosphorus Chemistry & Chemical Biology, Department of Chemistry, Tsinghua University, Beijing, 100084, China
[b] MOE Key Laboratory of Organic Optoelectronics and Molecular Engineering, Department of Chemistry, Tsinghua University, Beijing, 100084, China
[c] Department of Chemistry, Center for Nanotechnology and Institute of Biomedical Technology, Chung-Yuan Christian University, Chung-Li, 32023, Taiwan, ROC

ARTICLE INFO

Keywords:
Aggregation-induced emission
Mechanochromic materials
Lattice stability
Intermolecular interaction
Substitution site

ABSTRACT

The current research of mechanochromic molecules focused on different molecular skeletons and the types of functional groups, where the design ideas were limited. We have synthesized a group of cyano-modified TPE derivatives (**TPECN**) with different substitution sites, showing typical aggregation induced emission (AIE) effect. We found that meta-substituted **mCN** revealed the inertness of mechanochromism, whether being ball milled or rapidly evaporated. Isomers with ortho- or para-substitution showed an emission wavelength shift over 40 nm. Experimental data indicated unusual high-strength lattice stability for **mCN**. By single-crystal analysis and theoretical calculations, we clarified from the molecular skeleton distortion, noncovalent intermolecular interactions, and calculated interaction energy that the meta-substitution led to a stable lattice structure, making **mCN** insensitive to external stimuli. Thus, we successfully explained the substituted site was an important and independent factor that influenced the mechanochromic property. Meanwhile, we also explored the application of the **TPECN**s series for erasable printing and coding.

1. Introduction

Fluorescent materials play an important role in modern society due to their eye-catching phenomenon and extensive applications [1–4]. Some of fluorophores exhibit morphology-dependent emission, specifically as a red-shift under external mechanical operations such as grinding, rubbing, and pressing, named mechanochromism (MC) [5–7]. It's generally believed that the lattice structure of mechanochromism materials transforms under the external mechanical stimuli, including the crystal-amorphism phase transition or the interconvert between different crystallographic forms, thus the fluorescence color could reversibly switch without changes in chemical structure [8–10]. Nowadays, mechanochromism materials have been widely researched and utilized as anti-counterfeiting coating, information encryption, pressure sensors, and stress damage visualization [11,12].

Mechanochromism materials are required to emit in the solid state in most cases due to the limitations of mechanical stimuli. However, the phenomenon of aggregation-caused quenching (ACQ) happens for most traditional fluorophores [13], [–] [17] which has seriously restricted their applications in the solid state or concentrated solutions, including the further research of mechanical responsiveness. In 2001, Tang's group reported a novel work of aggregation-induced emission (AIE) effect received great attention. AIE-active luminogens (AIEgens) exhibit intense fluorescence in the aggregated or solid state but emits weak or even no fluorescence in dilute solutions [18]. AIEgens, especially the tetraphenylethylene (TPE) derivatives [19], [–] [23] open a brand new approach and dimension for the research of mechanochromism behavior. Based on different molecular arrangements and packing modes, MC AIEgens, which emit a variety of luminous colors in the solid state, have been discovered or synthesized. Tang B Z. and Dong Y P. reported a series of TPE molecules modified with alkoxy groups (such as ethoxy and n-butoxy) with a red-shift of over 40 nm during the crystalline-amorphous phase transition [24]. Through the two-phase reversible transformation, the reversible control of the fluorescence color and intensity could be realized. Jun Y. L. conducted an in-depth study on the influence of different groups on the mechanochromic properties, including common functional groups such as methyl, trifluoromethyl, and cyano [25]. Substitution site is a less researched factor at present due to the great steric hindrance of ortho and meta sites, which makes TPE derivatives with ortho/meta-modify show

* Corresponding author. The Key Laboratory of Bioorganic Phosphorus Chemistry & Chemical Biology, Department of Chemistry, Tsinghua University, Beijing, 100084, China.
E-mail address: weiyen@tsinghua.edu.cn (Y. Wei).

https://doi.org/10.1016/j.dyepig.2021.109939
Received 24 September 2021; Received in revised form 8 November 2021; Accepted 8 November 2021
Available online 22 November 2021

disadvantages in terms of yield and post-synthesis. Most of the MC AIEgens focus on para-modification [26–29]. Li B. S. once reported a case of differences in MC phenomenon caused by amino modification at different substitution sites [30]. Regarding whether the substituted sites influence the MC property, it is difficult to conclude at present due to the limited amount of experimental phenomena and data, and it also brings uncertain factors to the design and synthesis of MC AIEgen.

Here we've synthesized three isomers through the attachment of cyano-group into different substitution sites of TPE skeleton, named **oCN**, **mCN**, and **pCN**. The differences in the crystal structure, packing mode, and interaction energy of three isomers caused them different in response to external stimuli. Meta-substitution resulted in more stable stacking with lower energy, which led to the inertness of mechanochromism for **mCN**. Fluorescence wavelength switch in different solid states and theoretical calculations supported this view. Message encryption and erasure applications were also explored by the combination of these three isomers successfully.

2. Results and discussion

2.1. Synthesis and characterization of TPECNs

As shown in Fig. S1, **TPECN**s (including **oCN**, **mCN**, and **pCN**) were synthesized from differently substituted cyanophenyl boronic acids for the first time by a one-step coupling reaction with a satisfactory yield [31]. All compounds were characterized by nuclear magnetic resonance (NMR) (Figs. S2–S7) and high-resolution mass spectrometry (HRMS). FT-IR spectra provided strong evidence for cyanophenyl structure in**TPECN**s (Fig. S8). The proposed structures are also in agreement with elemental analysis and X-ray single-crystal diffraction (XRSD) results. Thermogravimetric analysis (TGA) revealed all three species of **TPECN**s were thermally stable with decomposition temperatures over 250 °C (Fig. S9). The dipole moments were calculated as 4.01, 5.08, and 5.56 Debye for **oCN**, **mCN**, and **pCN** by density functional theory (DFT) (see Fig. 1).

The optical properties of **TPECN**s were measured by UV–vis absorption and fluorescence spectroscopy. **oCN** and **mCN**in ethyl acetate solution exhibited an absorption peak located at around 300 nm, while **pCN** showed a red-shifted absorption peak at 323 nm (Fig. 2a), revealing

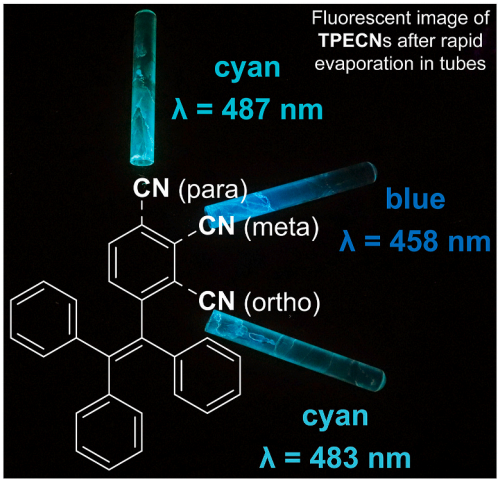

Fig. 1. AIE-active isomers in this work.TPECNs with different substituted-sites had different crystal structures and intermolecular van der Waals force. The intermolecular interaction between **oCN** and **pCN** was weaker than **mCN**, and **mCN** showed stronger aggregation and crystallization tendency, resulting in the inertness of mechanochromism for **mCN** out of three isomers. The digital image showed **TPECN**s films produced by rapid evaporation with visually disparate fluorescence wavelengths under UV irradiation, although their emission wavelengths in the crystal state were nearly identical.

a more conjugated structure in **pCN** probably due to the para-substitution. On the other hand, all species of **TPECN** possessed an AIE-active feature which is identical to many TPE derivatives [32,33]. As shown in Fig. 2b, **oCN**, **mCN**, and **pCN** behaved as a faint emitter in THF solution and no obvious change when f_w less than 70%. The fluorescence intensity increased significantly with further addition of water, suggesting that **oCN**, **mCN**, and **pCN** were all typical AIE-active luminogens (Figs. S10–S12). In particular, **mCN** reached the aggregation state earlier than **oCN** and **pCN** during the transition from THF to the water phase, suggesting the stronger interactions and the more compact packing for **mCN**.

2.2. Mechanochromism of TPECNs

Many AIEgens showed morphology-dependent luminescence switched between the crystal and amorpphis form. As shown in Figs. 3a–5a, during usual lattice-destruction operations [34–36] like grinding, ball-milling or melting to amorpphis, both **oCN** and **pCN** exhibited significant fluorescence red-shift (from blue to cyan). For **mCN**, despite what kind of lattice-destruction operations could not achieve mechanochromism phenomenon. Then the photophysical properties were further characterized, showed in Figs. 3b–5b and Table 1 **oCN** and **pCN** emitted cyan fluorescence peaked around 485 nm, which was over 40 nm spectral red-shift compared with their crystal form. **mCN** in different forms showed negligible shift of only 2 nm and no visible color change. The solid-state fluorescence quantum yields (PLQY) in the crystal state were respectively 0.154, 0.389, and 0.533 for **oCN**, **mCN**, and **pCN**. There was no obvious fluorescence intensity attenuation or quenching from the crystal to the amorphous state (shown in Table 1), indicating no obvious crystallization-induced emission enhancement (CIEE) effect in **TPECN**s [37–39]. Besides, the emission shift of **oCN** and **pCN** could be reversibly recovered by thermal annealing or solvent fumigation as recrystallization, which was consistent with the mechanochromism phenomena previously reported.

So there were two possible factors contributing to the inertness of mechanochromism behavior for **mCN**: the inability of usual lattice-destructions on **mCN** crystal, or the intrinsic absence of morphology-dependent luminescence for **mCN**. Further structure studies were conducted by differential scanning calorimetry (DSC) and powder X-ray diffraction (PXRD). As shown in Figs. 3c–5c, no other peaks were shown in the DSC thermograms of the original **oCN** and **pCN** except the melting peak. However, a significant exothermic peak appeared after grinding, at 77 °C (**oCN**) and 60 °C (**pCN**) respectively, indicating an amorphis-crystal phase transition. For **mCN** after ground there did not exist an exothermic peak, which indicated neither grinding nor melting could cause **mCN** to transform and remain in the amorphous state, thus showing fluorescence consistent with its crystal state. The PXRD provided more direct evidence. By comparing the PXRD patterns of the original state, the ground state, the fumed state, and the single crystal, it could be found the microstructure switch of **TPECN**s shown in Figs. 3d–5d. The original and fumed states of three kinds of **TPECN**s showed the same diffraction peaks as each single crystal, indicating the microstructures of **TPECN**s were crystalline both at the time of preparation and after annealing or fuming. The PXRD patterns of ground **oCN** and **pCN** were further scrutinized. Through grinding or melting, part of the diffraction peaks for **oCN**, such as $2\theta = 13.42°$ (111), 15.74° (120), 19.36° (121), and for **pCN**, such as $2\theta = 11.14°$ (010), 13.88° (012), 16.74° (013), 21.02° (112) became weakened or even disappeared. Upon the same operations, ground **mCN** powder still showed abundant diffraction peaks which had existed in the crystal state, as $2\theta = 9.10°$ (001), 12.90° (011) and 18.98° (111), indicating an intact crystal structure kept after grinding. So **mCN** was insensitive to usual lattice-destructions like grinding or melting, whereas the lattice of **oCN** and **pCN** had been damaged thus exhibiting mechanochromism behavior.

In conclusion, although **oCN**, **mCN**, and **pCN** were all cyano-substituted TPE derivatives with different substitution sites only, they

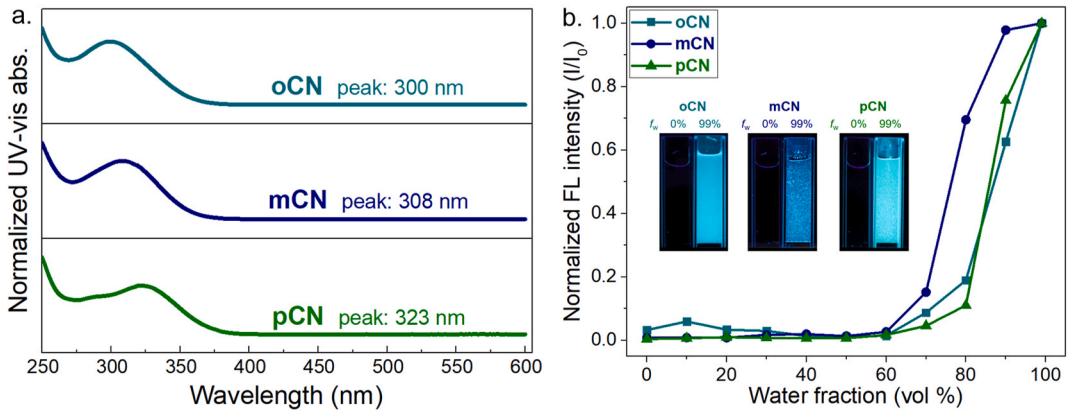

Fig. 2. Absorption and emission properties of TPECNs. (a) The UV–vis absorption spectra of **oCN**, **mCN**,and **pCN** in ethyl acetate solutions (0.5 mg mL^{-1}). (b) Plot of the normalized fluorescence intensity of **oCN**, **mCN**, and **pCN** with different THF/water fractions excited at 300 nm, where I_0 is the FL peak intensity in water. Inset shows the photograph of solutions of **TPECN**s at different THF/Water compositions upon exposure to UV light.

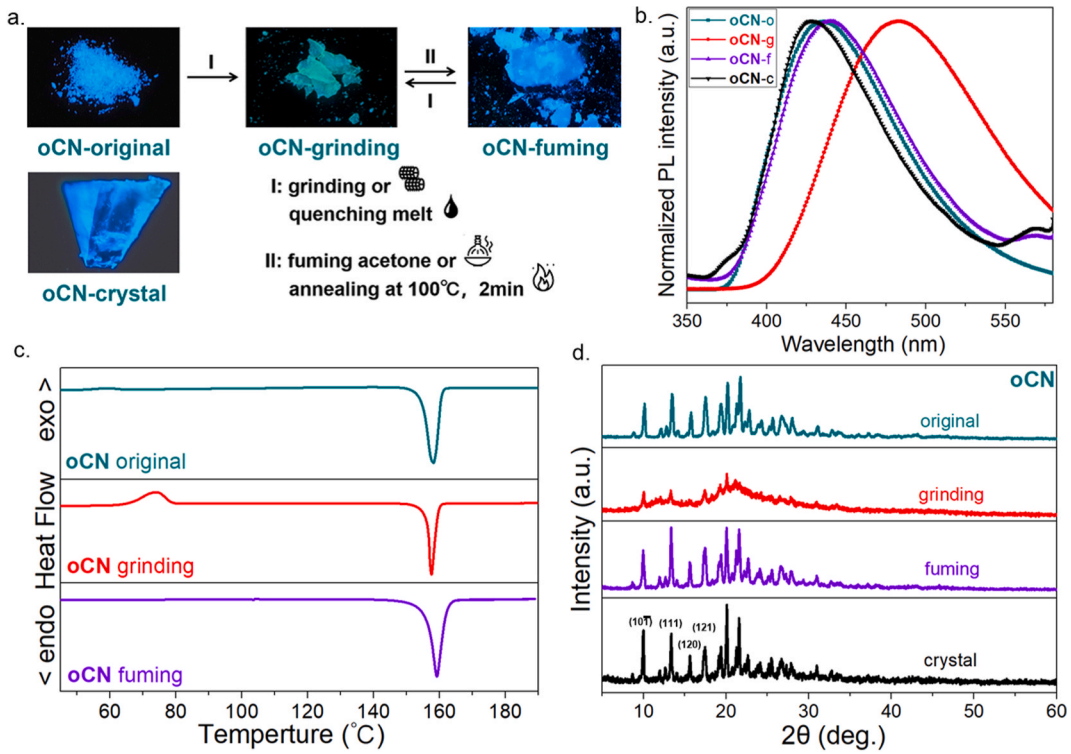

Fig. 3. Mechanochromism property and characterization of oCN. (a) Digital images of o**CN** in different states, including the original powder, ground powder, fumed powder, and crystal taken under UV illumination. (b) The emission spectra of oCN in different states excited at 300 nm. (c) DSC thermograms and (d) Powder X-ray diffraction (PXRD) patterns of oCN in different states.

still had completely different mechanochromism properties. In other words, in the case of the same molecular formula and functional groups, the substitution site was also an independent factor influencing mechanochromism. Compared with **oCN** and **pCN**, the lattice of **mCN** showed higher resistance and lattice stability to grinding and melting quenching, which might be related to the crystal properties of **mCN**.

2.3. Single-crystal structures of TPECNs

The single-crystal X-ray diffraction was conducted to analyze the structural features of **TPECN**s. The crystals of all three species were prepared by recrystallization of the methanol/water (v/v = 9/1) solution. The temperature stepped dropped from 90 to 0 °C, to result in rhombus-shaped crystals of **oCN** and needle-shaped crystals of **mCN** and **pCN** (detailed information listed in Table S1). The molecular geometry of **TPECN**s was highly twisted between phenyl rings and vinyl core (Fig. 6a–c). Through the analysis of dihedral angles, **mCN** had the slightest twist, while **oCN** and **pCN** larger (almost all dihedral angles were above 50 deg.). The larger torsion in crystal structures meant that the rotational space could be compressed during the crystal-amorphous transition, resulting in an emission shift. Relevant studies had pointed out that a planar conformation may lead to the mechanochromism inertness which was completely consistent with the phenomenon observed here.

From the previous words, there is no correlation between dipole moments and mechanochromism behavior for **TPECN**s, so we temporarily ignore the electrostatic orientation but focus on the noncovalent intermolecular interactions in the crystalline state including C–H···N

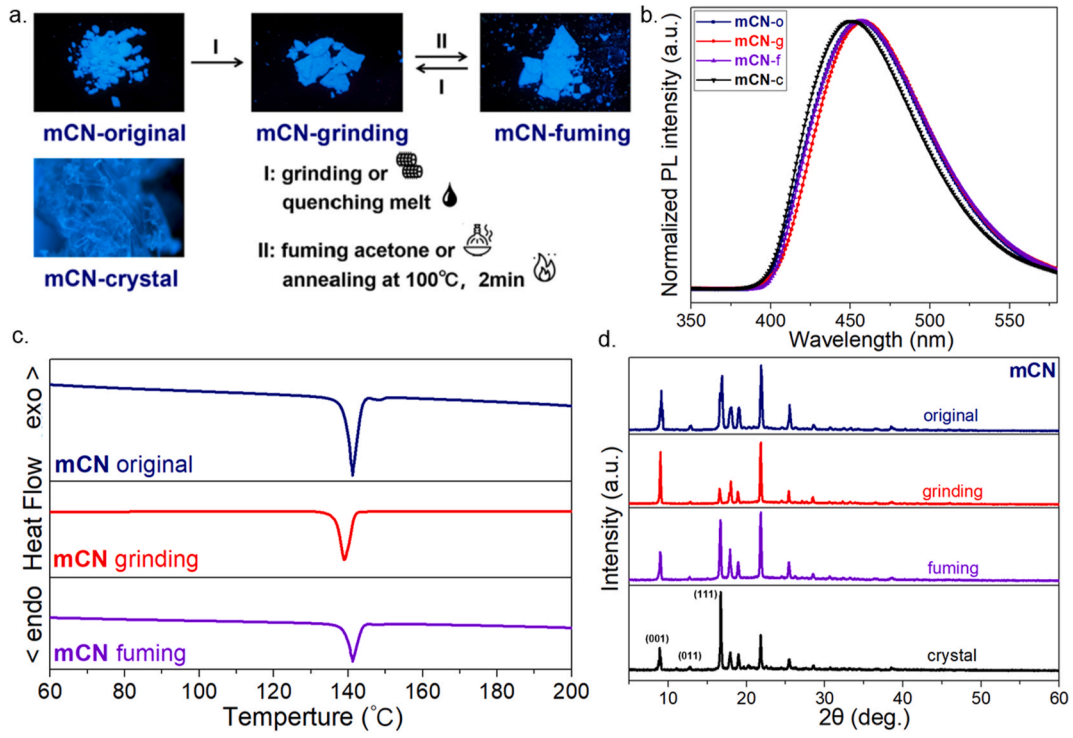

Fig. 4. Mechanochromism property and characterization of mCN. (a) Digital images of **mCN** in different states, including the original powder, ground powder, fumed powder, and crystal taken under UV illumination. (b) The emission spectra of **mCN** in different states excited at 300 nm. (c) DSC thermograms and (d) Powder X-ray diffraction (PXRD) patterns of mCN in different states.

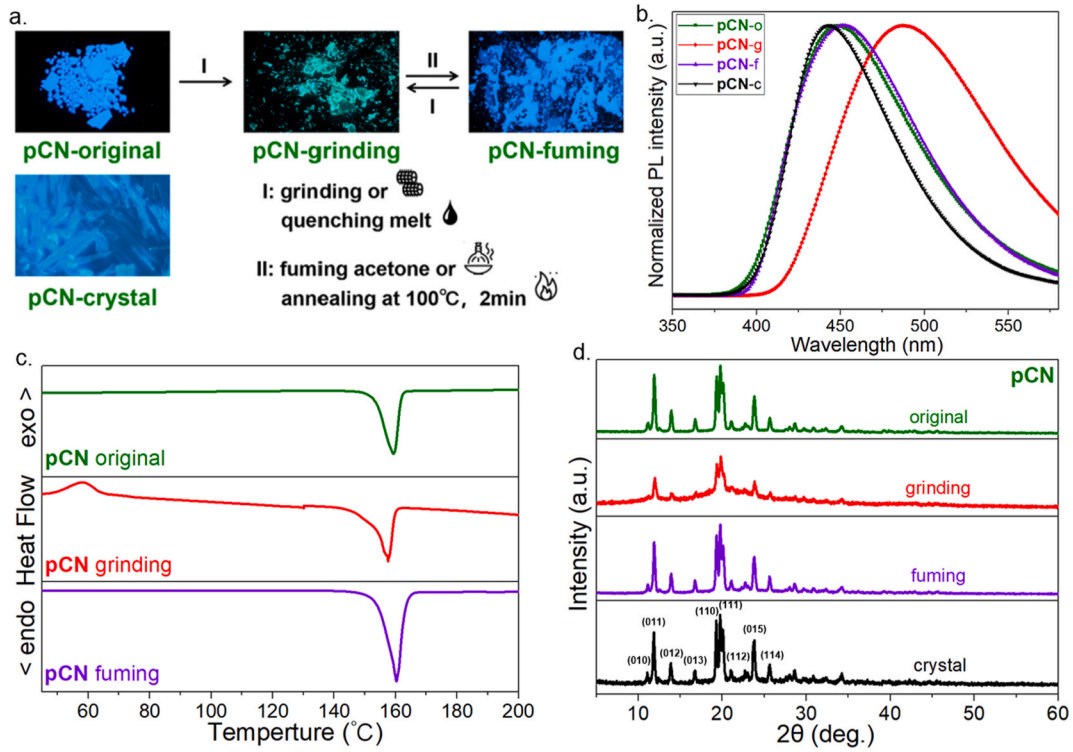

Fig. 5. Mechanochromism property and characterization of pCN. (a) Digital images of **pCN** in different states, including the original powder, ground powder, fumed powder, and crystal taken under UV illumination. (b) The emission spectra of **pCN** in different states excited at 300 nm. (c) DSC thermograms and (d) Powder X-ray diffraction (PXRD) patterns of **pCN** in different states.

Table 1
Emission and mechanochromism property of solid TPECNs in different forms.oCN and **pCN** showed a conspicuous and reversible emission shift (from blue to cyan) after grinding while **mCN** yet. ***o*** for the original powder, ***g*** for the ground powder, ***f*** for the fumed powder, and △λ for the grinding-induced emission shift.

Compounds	Emission Wavelength λ (nm) (PLQY)			△λ (nm)
	o	G	f	
oCN	436 (0.154)	483 (0.123)	440 (0.147)	47
mCN	456 (0.389)	458 (0.377)	457 (0.398)	2
pCN	447 (0.533)	487 (0.452)	451 (0.512)	40

and C–H … π weak hydrogen bonds. Table S1 and Fig. 6d–f showed all intermolecular interactions within 3.3 Å distance in the crystals of three **TPECN**s. It was obvious that the quantity of possible weak hydrogen bonds between **mCN** molecules was the most and the distance was the shortest (all within 3.11 Å), indicating greater interactions and a more stable lattice structure. In contrast, the intermolecular interactions between **oCN** and **pCN** were slightly weaker, especially C–H … π bond was found only a distant one in **oCN** crystal, and even absent in **pCN** crystal. However, it's an extensive and important interaction in TPE derivatives. Thus, the ordered packing and tight interactions caused **mCN** a greater resistance to lattice-destruction than **oCN** and **pCN**, resulting in the inertness of mechanochromism.

In addition to specific weak hydrogen bonds related to molecular conformation, the general interaction energies between molecules had been calculated and compared, since they also exerted an important effect on the stability of the crystal structure. Weaker intermolecular interactions may still exist in the amorphous form, or be compensated for by greater van der Waals dispersion between closer adjacent molecules, so we focused here on the three nearest molecule pairs in the crystal state. Through the analysis of single-crystal structure, it was conspicuous that the central molecule of **oCN** had only one closest adjacent molecule (distance: 6.902 Å), 2 s-closest, and two third-closest adjacent molecules (distance: 8.318 Å and 8.364 Å, respectively). And the central molecule of **mCN** had two closest adjacent molecules at a distance of 7.231 Å, as well as 2 s-closest and two third-closest adjacent molecules (distance: 8.833 Å and 9.182 Å, respectively). The structure of **pCN** was the loosest than other isomers, the central molecule had two closest (distance: 7.947 Å), 4 s-closest (distance: 9.103 Å), and two third-closest (distance: 9.441 Å) adjacent molecules.

Through Symmetry-Adapted Perturbation Theory, the interaction energy between the closest molecular pairs in **TPECN**s was calculated to further explain the contribution of intermolecular interactions to structural stability out of these three isomers (Fig. 7d). The calculation results showed that the closest molecule pair in the **oCN** crystal possessed an interaction energy of −12.0 kcal/mol and that in the **mCN** crystal was −12.7 kcal/mol. The two values were not much different, but there were two identical closest molecular pairs in **mCN** which provided significantly stronger interactions. The interaction energy of the closest molecular pair of **pCN** was only −9.2 kcal/mol (see Table S2 for specific calculation parameters). **mCN** had the lowest interaction energy among three isomers, which could enhance the stability of the crystal lattice and firmly resist external stimuli. On the other hand, the calculation results showed the interaction energy was not exactly consistent with the molecular distance, indicating that apart from the distance-related London dispersion force, there were other directional polar effects, which further confirmed the rationality of weak hydrogen bonds analyzed in the previous section. The interaction energy of the second- and third-closest molecular pairs for **TPECN**s were also calculated in Table S3. The interaction energy provided by the more distant molecules is less and less important for stabilizing the lattice structure, but still of some reference value.

According to the analysis of single-crystal structures, considering the distortion of molecular conformation, the weak hydrogen bonds between molecules and the calculated interaction energy data, it could be found that **mCN** had a tighter stacking mode, numerous weak interactions, and lower interaction energy due to meta-substitution, which caused **mCN** a more stable lattice structure to resist external stimuli. This could be thought of as the origin of the difference in mechanochromism behavior from **TPECN**s.

2.4. Applications of TPECNs

We explored the application in erasable ink and optical recording through the combination of three **TPECN**s after studying the mechanism. The difference in mechanochromism response between **oCN**/**pCN** and **mCN** could be utilized to load and store information. After printing the **TPECN**s-dissolved ink on the paper and natural evaporation, we found that **oCN** and **pCN** emitted cyan fluorescence under the UV light,

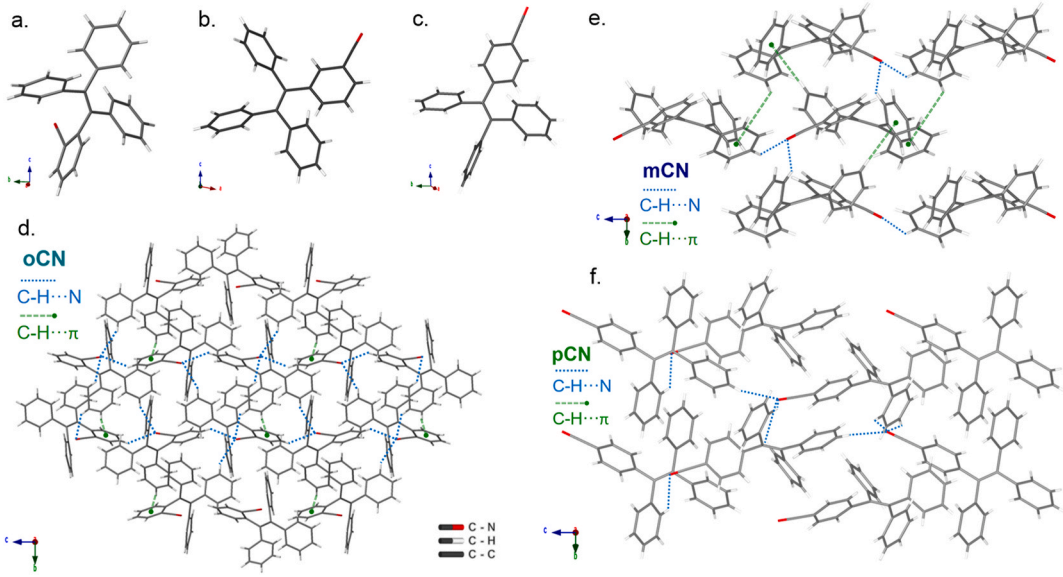

Fig. 6. Crystal structures and molecular conformations of TPECNs. The molecular structure and conformation of (a) **oCN**, (b) **mCN**, and (c) **pCN** analyzed from X-ray single-crystal diffraction (XRSD). Molecular packing and intermolecular interactions in the crystal of (d) **oCN**, (e) **mCN**, and (f) **pCN** viewed down the *a* axis where blue dotted lines representing C–H···N weak hydrogen bond and green dotted lines for C–H … π weak hydrogen bond.

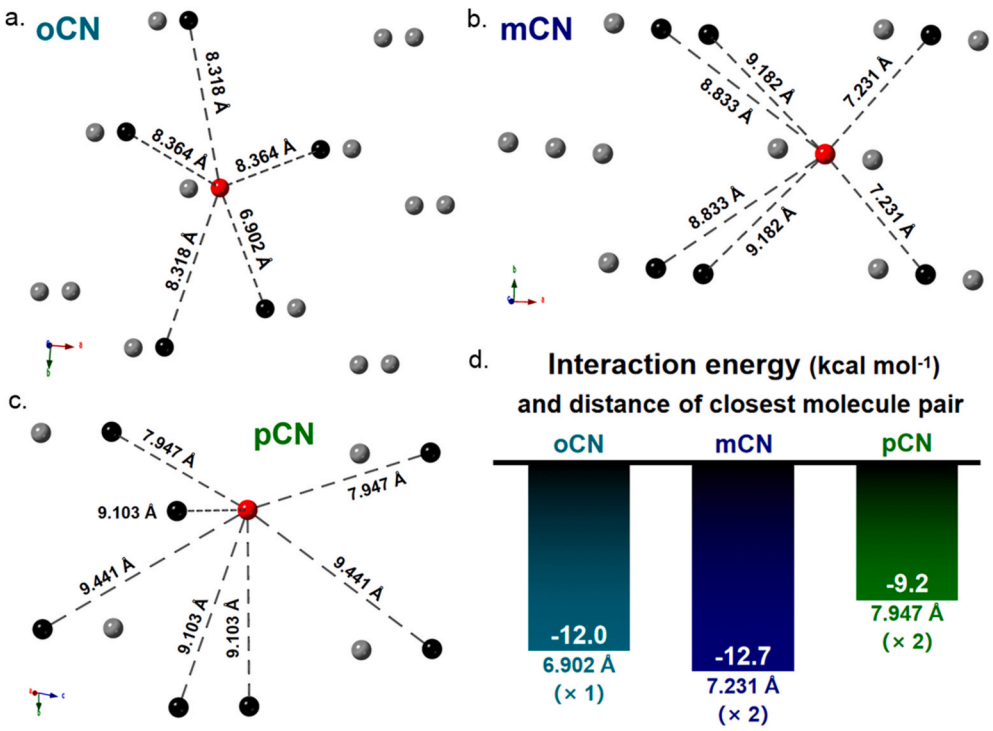

Fig. 7. The distance and interaction energy between adjacent molecules in the crystal of TPECNs. The distance between the central molecule (marked in red) and its neighbors was studied using a simplified model of the molecule's mass center, for **oCN** (a), **mCN** (b), and **pCN** (c). One of the second-closest molecule pairs was outside the image range and not displayed here. The distance between the closest, second-closest, and third-closest (marked in black) adjacent molecules were also signed. The closest adjacent molecule provided the most important intermolecular interactions so the interaction energy of **TPECN**s was calculated and compared with each other (d).

which was unique for the amorphous state, while **mCN** emitted blue. After heating the printed paper for a while, the three isomers were all annealed to blue emission as the crystal state, which was difficult to identify. Through the difference in mechanochromism property between three **TPECN**s, the marking and erasure of specific highlighting in the text could be achieved. In Fig. 8a, the 'Janu' in the text 'Janus' was especially marked but then lost specificity after annealing, which meant the erasure of extra information.

In addition to using two kinds of **TPECN**s for the text printing and highlighting, erasable coding in one character could also be realized. As shown in Fig. 8b, the digital display system of Arabic numerals adopted mixed coding by two kinds of **TPECN**s, in which **oCN** or **pCN** was printed in the emission area of a specific number (the number '2' in Fig. 8b), and other parts were filled with **mCN**. After the dye annealed, the entire character emitted blue fluorescence, realizing the erasure of information. Based on this design, we tried the erasable coding of ten Arabic numerals. The results were shown in Fig. 8c that all numerals could be mixed coded by two kinds of **TPECN**s, the coded paper had no traces under sunlight and successfully showed cyan numerals under UV irradiation. Next, annealing made the cyan parts of each numeral

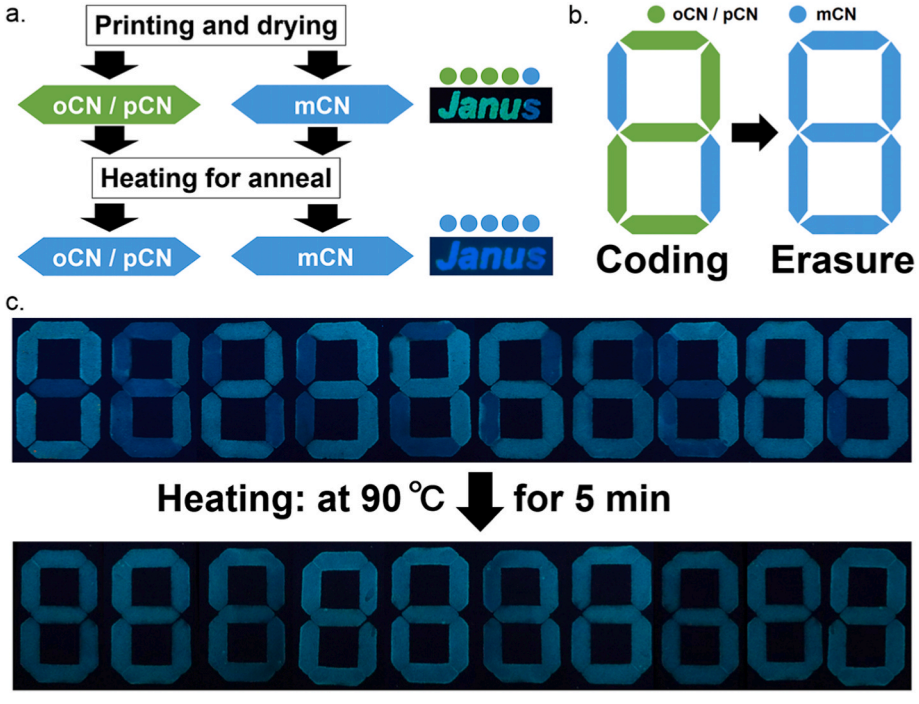

Fig. 8. Applications of TPECNs. (a) The morphology-dependent emission of **TPECN** isomers used in printing. **oCN** and **pCN** showed cyan emission after printing, and switched to blue after heating and annealing, while **mCN** was blue all the way. The combination could be utilized for text printing and erasable highlighting information. (b) Mixed encoding and erasure of single characters. (c) Encoding and erasing experiments on 10 Arabic numerals verified the application of **TPECN**s for reversible information storage and erasure. All images were taken under UV irradiation.

disappear, and no specific number could be read again. Besides, the cyclic stability of **TPECN**s between the crystal and amorphous states was also researched. Both **oCN** and **pCN** achieved significant switches in wavelength during four complete crystal-amorphis cycles, while the emission of **mCN** in this process keeping at a stable wavelength (Fig. S13), which also improved the application efficiency and value of **TPECN**s.

3. Conclusion

Using a group of cyano-modified TPE derivatives with the same functional group and the molecular formula but different substitution sites, we've successfully observed the difference of meta-substituted **mCN** from the other two isomers with the inertness of mechanochromism property. By the single crystal analysis and theoretical calculations, it was found that the meta-substitution mode caused the slighter distortion for molecular conformation, the tighter stacking mode, the more numerous interactions, and the lower interaction energy out of three **TPECN**s, which enhanced the lattice stability of **mCN** and made it insensitive to external stimuli. In contrast, **oCN** and **pCN** displayed visible and reversible emission shifts over 40 nm. The combination of three **TPECN**s had promising applications and great impetus in the erasable printing and coding. This work enriched the evidence that the site of substitution could be regarded as an independent and important factor to influence mechanochromism behavior. The potential 'meta-site effect' provided a new perspective for the molecular design of mechanochromism materials and facilitated a deeper understanding on the mechanism of mechanochromism.

4. Methods

4.1. Materials and procedures

The carbon-carbon coupling reaction was performed following previously published procedures. All the commercially available chemicals and solvents were used directly without further purification. Reactions were monitored using thin-layer chromatography (TLC) with commercial TLC plates. Products were isolated by silica gel column chromatography.

4.2. Instrumentation

All ^{1}H and ^{13}C NMR spectra were recorded in DMSO-d_6 solutions at 298K using a Bruker (400 MHz) spectrometer with tetramethylsilane (TMS) as an internal standard. Mass spectra were recorded on HRMS, Performance (Shimadzu, Japan). Perkin Elmer CE-440 was used for micro elemental analyses. Infrared spectra were recorded by Perkin Elmer (Spectrum 100) FT-IR Spectrometer. UV–visible spectra were recorded using Perkin Elmer (Lambda 750) UV/Vis/NIR Spectrometer in ethyl acetate solvent. Fluorescence emission and quantum yield measurements were performed by SHIMADZU Spectro fluorophotometer RF-6000. Thermogravimetric analysis were performed on BeiguanghongyuanWCT-12. Differential scanning caborimetry were performed on TA Instrument DSC 2000. Wide-angle X-ray powder diffractions were performed by Rigaku D/max-2550.

4.3. Single crystal studies

Single crystals of oCN, mCN, and pCN were prepared by recrystallization of the methanol/water (v/v = 9/1) solution at a stepped temperature range from 90 to 0 °C. The solution concentrations in the growing conditions were 5 mg mL^{-1} for oCN, 10 mg mL^{-1} for mCN, and 5 mg mL^{-1} for pCN. The structures of single-crystal were determined at 150K by Rigaku Oxford diffraction system with a CCD detector and graphite-monochromated Cu Kα radiation. The crystallographic data for TPECNs (CCDC no. 2071238 for oCN, 2071239 for mCN, and 2071237 for pCN, respectively) (CIF) were shown as supplementary materials.

4.4. Synthesis of TPECN compounds

2-(1,2,2-triphenylvinyl)benzonitrile (**oCN**) was synthesized by Suzuki-Miyaura coupling with a final yield of 43.6%.M.p. 158–159 °C. ^{1}H NMR (400 MHz, DMSO-d_6):δ7.61 (d, J = 7.8 Hz, 1H, of the cyanophenyl ring), 7.50 (t, J = 7.6 Hz, 1H, of the cyanophenyl ring), 7.37–7.26 (m, 2H, of the cyanophenyl ring), 7.17–6.92 (m, 15H, of three benzene rings). ^{13}C NMR (101 MHz, DMSO-d_6): δ147.35, 144.63, 142.64, 142.52, 141.49, 137.46, 133.36, 133.33, 132.53, 130.99, 130.81, 130.73, 128.58, 128.53, 128.23, 127.72, 127.65, 127.55, 118.68, 113.17. HRMS (ESI): calcd for $C_{27}H_{19}N$ [M + Na]$^{+}$, 380.1410; found, 380.1408. Anal. calcd for $C_{27}H_{19}N$: C, 90.72; H, 5.36; N, 3.92%. Found: C, 90.195; H, 5.335; N, 4.033%.

3-(1,2,2-triphenylvinyl)benzonitrile (**mCN**) was synthesized by Suzuki-Miyaura coupling with a final yield of 87.8%.M.p. 141–142 °C. ^{1}H NMR (400 MHz, DMSO-d_6): δ 7.51 (p, J = 4.6 Hz, 1H, of the cyanophenyl ring), 7.33 (s, 1H, of the cyanophenyl ring), 7.27 (d, J = 4.6 Hz, 2H, of the cyanophenyl ring), 7.14–6.92 (m, 15H, of three benzene rings). ^{13}C NMR (101 MHz, DMSO-d_6): δ 145.07, 143.03, 142.96, 142.92, 142.67, 139.05, 135.98, 134.61, 131.23, 131.07, 130.74, 129.68, 128.57, 128.40, 127.52, 127.47, 127.42, 119.06, 111.54. HRMS (ESI): calcd for $C_{27}H_{19}N$ [M + Na]$^{+}$, 380.1410; found, 380.1407. Anal. calcd for $C_{27}H_{19}N$: C, 90.72; H, 5.36; N, 3.92%. Found: C, 90.410; H, 5.368; N, 4.009%.

4-(1,2,2-triphenylvinyl)benzonitrile (**pCN**) was synthesized by Suzuki-Miyaura coupling with a final yield of 83.4%.M.p. 159–160 °C. ^{1}H NMR (400 MHz, DMSO-d_6): δ 7.54 (d, J = 8.1 Hz, 2H, of the cyanophenyl ring), 7.15–6.92 (m, 17H, of the cyanophenyl ring and three benzene rings). ^{13}C NMR (101 MHz, DMSO-d_6):δ 148.91, 143.17, 143.05, 142.92, 142.75, 139.62, 132.27, 132.16, 131.22, 131.09, 128.60, 128.40, 127.66, 127.48, 119.25, 109.57. HRMS (ESI): calcd for $C_{27}H_{19}N$ [M + Na]$^{+}$, 380.1410; found, 380.1408. Anal. calcd for $C_{27}H_{19}N$: C, 90.72; H, 5.36; N, 3.92%. Found: C, 90.482; H, 5.387; N, 4.030%.

5. Computational methods

The dipole moments were calculated at optimized geometry of the ground state of the corresponding single molecular in gas phase using density functional theory (DFT) method with B3LYP functional and basis set is 6–31g(d). The cartesian coordinates for single molecular of three isomers were shown in the Supplementary Information.

The interaction energy between the selected two molecules/fragments in the crystal was calculated through Symmetry-Adapted Perturbation Theory (SAPT) [40] implemented in Q-Chem [41] without considering Møller-Plesset fluctuation operators for both two fragments (SAPT0) [42]. Electronic structure used for SAPT calculation was obtained by density functional theory (DFT) carried out using cam-b3lyp functional and the basis set is def2-tzvpp. The structure of the two fragments and their relative position used for calculation were directly adopted from XRSD results.

Data availability

The data supporting the finding of this study are available in the article and Supplementary Information, or from the lead contact upon reasonable request.

Further information and requests for resources and reagents should be directed to and will be fulfilled by the lead contact, Yen Wei (weiyen@tsinghua.edu.cn).

oCN, **mCN**, and **pCN** generated in this research will be made available on request, but we may need payment and/or a completed Materials Transfer Agreement if there is potential for commercial application.

Code availability

The codes supporting the computational studies of this study are available in the Supplementary Information, or from the lead contact upon reasonable request.

CRediT authorship contribution statement

Mengshi Wang: carried out the synthesis, characterization and other experimental work, wrote the paper with input from all authors. **Yuanheng Wang:** performed the theoretical calculation and analysis, wrote the paper with input from all authors. **Renjian Hu:** wrote the paper with input from all authors. **Ruoxin Li:** wrote the paper with input from all authors. **Zhigang Shuai:** conceived and supervised the project. **Yen Wei:** conceived and supervised the project.

Declaration of competing interest

The authors declare that they have no known competing financial interests or personal relationships that could have appeared to influence the work reported in this paper.

Acknowledgements

This work was supported by the National Natural Science Foundation of China (Nos. 21788102). We are most grateful to Danning Hu, Liucheng Mao, and Hongye Huang of Tsinghua University for valuable assistance and suggestions.

Appendix A. Supplementary data

Supplementary data to this article can be found online at https://doi.org/10.1016/j.dyepig.2021.109939.

References

[1] Shi H, et al. Real-time monitoring of cell apoptosis and drug screening using fluorescent light-up probe with aggregation-induced emission characteristics. J Am Chem Soc 2012;134:17972–81.
[2] Li Q, et al. Unusual light-driven amplification through unexpected regioselective photogeneration of five-membered azaheterocyclic AIEgen. Chem Sci 2021;12:709–17.
[3] Jiang X, et al. Highly-sensitive optical organic vapor sensor through polymeric swelling induced variation of fluorescent intensity. Nat Commun 2018;9:1–9.
[4] Rosenberg M, et al. Design, synthesis, and time-gated cell imaging of carbon-bridged triangulenium dyes with long fluorescence lifetime and red emission. Chem Sci 2018;9:3122–30.
[5] Nagura K, et al. Distinct responses to mechanical grinding and hydrostatic pressure in luminescent chromism of tetrathiazolylthiophene. J Am Chem Soc 2013;135:10322–5.
[6] Chen XW, et al. Mechanochromic luminescent materials of bimetallic Cu(i) complexes showing thermally activated delayed fluorescence. J Mater Chem C 2020;8:16160–7.
[7] Wei YC, et al. Mechanochromism induced through the interplay between excimer reaction and excited state intramolecular proton transfer. Commun. Chem. 2019;2:1–9.
[8] Kuroda Y, et al. Observation of crystallisation dynamics by crystal-structure-sensitive room-temperature phosphorescence from Au(I) complexes. Commun. Chem. 2020;3:1–8.
[9] Echeverri M, et al. Untangling the mechanochromic properties of benzothiadiazole-based luminescent polymorphs through supramolecular organic framework topology. J Am Chem Soc 2020;142:17147–55.
[10] Xu B, et al. Achieving remarkable mechanochromism and white-light emission with thermally activated delayed fluorescence through the molecular heredity principle. Chem Sci 2016;7:2201–6.
[11] Zhao Y, et al. Crosstalk-free patterning of cooperative-thermoresponse images by the synergy of the AIEgen with the liquid crystal. Angew Chem Int Ed 2020;59:10066–72.
[12] Sun H, et al. Smart responsive phosphorescent materials for data recording and security protection. Nat Commun 2014;5:1–9.
[13] Mi BX, et al. Reduction of molecular aggregation and its application to the high-performance blue perylene-doped organic electroluminescent device. Appl Phys Lett 1999;75:4055–7.
[14] Lin WJ, Chen WC, Wu WC, Niu YH, Jen AKY. Synthesis and optoelectronic properties of starlike polyfluorenes with a silsesquioxane core. Macromolecules 2004;37:2335–41.
[15] Xiao S, et al. Stabilization of semiconducting polymers with silsesquioxane. Adv Funct Mater 2003;13:25–9.
[16] Sharma A, et al. Tuning photophysical and electroluminescent properties of phenanthroimidazole decorated carbazoles with donor and acceptor units: beneficial role of cyano substitution. Dyes Pigments 2021;184:108830.
[17] Domínguez R, Navarro A, García-Martínez JC. Styrylbenzene organogels and how the cyano groups tune the aggregation-induced emission. Dyes Pigments 2021;192:109427.
[18] Luo J, et al. Aggregation-induced emission of 1-methyl-1,2,3,4,5-pentaphenylsilole. Chem Commun 2001;18:1740–1.
[19] Wang X, et al. Exploiting radical-pair intersystem crossing for maximizing singlet oxygen quantum yields in pure organic fluorescent photosensitizers. Chem Sci 2020;11:10921–7.
[20] Zhang Y, Li J, Tang BZ, Wong KS. Aggregation enhancement on two-photon optical properties of AIE-active D-TPE-A molecules. J Phys Chem C 2014;118:26981–6.
[21] Ji J, Hu D, Yuan J, Wei Y. An adaptable cryptosystem enabled by synergies of luminogens with aggregation-induced-emission character. Adv Mater 2020;32:2004616.
[22] Shi J, et al. Switching emissions of two tetraphenylethene derivatives with solvent vapor, mechanical, and thermal stimuli. Chin Sci Bull 2013;58:2723–7.
[23] Xi W, et al. Photophysical switching between aggregation-induced phosphorescence and dual-state emission by isomeric substitution. Chem Eur J 2020;26:3733–7.
[24] Luo X, et al. Reversible switching emissions of tetraphenylethene derivatives among multiple colors with solvent vapor, mechanical, and thermal stimuli. J Phys Chem C 2012;116:21967–72.
[25] Jadhav T, et al. Effect of end groups on mechanochromism and electroluminescence in tetraphenylethylene substituted phenanthroimidazoles. J Phys Chem C 2016;120:18487–95.
[26] Xu B, et al. Very bright mechanoluminescence and remarkable mechanochromism using a tetraphenylethene derivative with aggregation-induced emission. Chem Sci 2015;6:3236–41.
[27] Wang J, et al. Click synthesis, aggregation-induced emission, E/Z isomerization, self-organization, and multiple chromisms of pure stereoisomers of a tetraphenylethene-cored luminogen. J Am Chem Soc 2012;134:9956–66.
[28] Tong J, et al. A 1,3-indandione-functionalized tetraphenylethene: aggregation-induced emission, solvatochromism, mechanochromism, and potential application as a multiresponsive fluorescent probe. Chem Eur J 2014;20:4661–70.
[29] Xiong J, et al. Multi-stimuli-Responsive fluorescence switching from a pyridine-functionalized tetraphenylethene AIEgen. ACS Appl Mater Interfaces 2018;10:5819–27.
[30] Jiang Y, et al. Insight from the old: mechanochromism and mechanoluminescence of two amine-containing tetraphenylethylene isomers. J Mater Chem C 2019;7:11790–6.
[31] Tobisu M, Chatani N. Devising boron reagents for orthogonal functionalization through suzuki-miyaura cross-coupling. Angew Chem Int Ed 2009;48:3565–8.
[32] Mei J, Leung NLC, Kwok RTK, Lam JWY, Tang BZ. Aggregation-induced emission: together we shine, united we soar. Chem Rev 2015:115 11718–11940.
[33] Mei J, et al. Aggregation-induced emission: the whole is more brilliant than the parts. Adv Mater 2014:26 5429–5479.
[34] Yu Y, et al. Stacking-induced different performance of mechanochromic luminescence and room-temperature phosphorescence based on two analogous AIEgens synthesized by a green photo-oxidation reaction. J Mater Chem C 2021;9:888–93.
[35] Jin M, Seki T, Ito H. Mechano-Responsive luminescence via crystal-to-crystal phase transitions between chiral and non-chiral space groups. J Am Chem Soc 2017;139:7452–5.
[36] Lavrenova A, et al. Mechano- and thermoresponsive photoluminescent supramolecular polymer. J Am Chem Soc 2017;139:4302–5.
[37] Hagihara R, et al. Push–pull bisnaphthyridylamine supramolecular nanoparticles: polarity-induced aggregation and crystallization-induced emission enhancement and fluorescence resonance energy transfer. Chem Eur J 2021;27:3039–46.
[38] Galer P, Korošec RC, Vidmar M, Šket B. Crystal structures and emission properties of the BF2 complex 1-phenyl-3-(3,5-dimethoxyphenyl)-propane-1,3-dione: multiple chromisms, aggregation- or crystallization-induced emission, and the self-assembly effect. J Am Chem Soc 2014;136:7383–94.
[39] Abdollahi MF, You J, Wang T, Zhao Y. Molecular tuning of the crystallization-induced emission enhancement of diphenyl-dibenzofulvene luminogens. Chem Commun 2021;57:484–7.
[40] Jeziorski B, et al. SAPT: a program for many-body symmetry-adapted perturbation theory calculations of intermolecular interaction energies. Methods Techn. Comput. Chem.: METECC 1993;*94* **B**:79.
[41] Shao Y, et al. Advances in molecular quantum chemistry contained in the Q-Chem 4 program package. Mol Phys 2015;113:184–215.
[42] Schäffer R, Jansen G. Intermolecular exchange-induction energies without overlap expansion. Theor. Chem. Accounts 2012;131:1–10.